Pergamon

Int. J. Heat Mass Transfer. Vol. 40, No. 7, pp. 1621–1631, 1997

0017–9310/97 $17.00+0.00

PII: S0017-9310(96)00192-5

Mixed convection heat and mass transfer in vertical rectangular ducts

KUAN-TZONG LEE and HON-LING TSAI

Department of Mechanical Engineering, Oriental Institute of Technology, Pan-Chiao, Taipei, Taiwan 22064, Republic of China

and

WEI-MON YAN

Department of Mechanical Engineering, Hua Fan College of Humanities and Technology, Shih-Ting, Taipei, Taiwan 22305, Republic of China

(*Received* 18 *January* 1996 *and in final form* 16 *May* 1996)

Abstract—The present study deals with the numerical prediction of mixed convection heat and mass transfer in a vertical rectangular duct with film evaporation along the porous wall. The Boussinesq approximation is invoked to take into account the buoyancy effect induced by thermal and mass diffusion. Computations are made here for the wetted wall temperature $T_w = 40°C$ and 60°C, relative humidity of moist air at the inlet $\phi = 10$, 50 and 90%, and the through-flow Reynolds number $Re = 1000$ and 2000. The numerical results, including the developments of velocity, temperature, concentration, Nusselt number, Sherwood number and friction factor, are presented. Predicted results show that the influences of the combined buoyancy force of thermal and solutal diffusion on the flow, heat and mass transfer are significant. Due to the film evaporation along the wetted wall, the mass transfer is found to enhance the heat transfer rate along the wetted wall. Additionally, the results disclose that the heat transfer along the wetted wall is predominated by the latent heat transfer connected with film vaporization. Copyright © 1996 Elsevier Science Ltd.

INTRODUCTION

Many transport processes exist in nature and industrial applications in which the transfer of heat and mass occurs simultaneously as a result of the combined buoyancy effects of thermal diffusion and diffusion of species. The processes occurring in nature include various photosynthetic mechanisms, discharge into bodies of water, calm-day evaporation and vaporization of mist and fog. The engineering applications include: the chemical reaction in a reactor chamber consisting of rectangular ducts, multirectangular-channel solar collectors, chemical vapor deposition of solid layers and cooling of electronic equipment.

Convection flows driven by temperature and concentration differences have been studied extensively in the past and various extensions of the problem have been reported in the literature. With both concentration and temperature interacting simultaneously, the convection flow can become quite complex. Combined heat and mass transfer along a vertical plate in natural convection flows have been studied in great detail. Somers [1] applied the integral method to investigate the problem of simultaneous heat transfer and binary diffusion of the driven flow adjacent to a wetted isothermal vertical surface in a non-saturated atmosphere; his result is valid only around Prandtl and Schmidt numbers of 1.0. Mather *et al.* [2] formulated the same problem in terms of boundary layer differential equations resulting from force-momentum, energy and chemical species concentration at very low concentration. Neglecting inertia effects, the resulting equations were solved by an analogue computer for $Pr = 1.0$ and $Sc = 0.5$–1.0 for the ratios of species and thermal diffusion buoyancy effects of 1.0 and 0.5. Gill *et al.* [3] gave an exact solution by the improved integral method for the nonlinear system of momentum, heat and binary mass transfer equations. The effects of variations of enthalpy, thermal conductivity, viscosity and density, with concentration were studied individually and in various combinations. Saville and Churchill [4, 5] analyzed the asymptotic process in terms of the Prandtl number and Schmidt number. The dependence of the transport parameters is found for $Pr = Sc \to 0$, for $Pr = Sc \to \infty$, for $Pr \to 0$ and $Sc \to \infty$ with $Sc \gg Pr$. Soundalgekar and Ganesan [6] investigated the unsteady characteristics of natural convection heat and mass transfer along a vertical plate. They concluded that the time required for the temperature field to reach the steady state is longer for the system with a higher Sc. Concerning the natural convection heat and mass transfer in vertical ducts, Lee *et al.* [7] deter-

NOMENCLATURE

A cross-sectional area of the vertical rectangular duct [m^2]
a channel width in the x-direction [m]
b channel width in the y-direction [m]
c mass fraction of water vapor
C dimensionless mass fraction of water vapor, $(c-c_0)/(c_w-c_0)$
D mass diffusivity [$m^2\ s^{-1}$]
D_e equivalent hydraulic diameter, $4A/S$, [m]
f friction factor, $2\bar{\tau}_w/(\rho\bar{w}_0^2)$
g gravitational acceleration [$m\ s^{-2}$]
Gr_t heat transfer Grashof number, $g\beta(T_w-T_0)D_e^3/\nu^2$
Gr_m mass transfer Grashof number, $g(M_a/M_v-1)(c_w-c_0)D_e^3/\nu^2$
h heat transfer coefficient [$W\ m^{-2}\ K^{-1}$]
h_{fg} latent heat of vaporization [$J\ kg^{-1}$]
h_m local mass transfer coefficient [$m\ s^{-1}$]
k thermal conductivity [$W\ m^{-1}\ K^{-1}$]
M number of finite difference divisions in the x-direction
M_a molecular weight of air [$kg/kmol^{-1}$]
M_v molecular weight of water vapor [$kg\ kmol^{-1}$]
N number of finite difference divisions in the y-direction
n dimensionless direction coordinate normal to the duct walls
Nu_l local Nusselt number (latent heat)
Nu_s local Nusselt number (sensible heat)
Nu_z overall Nusselt number $(=Nu_s+Nu_l)$
$\bar{p}$ cross-sectional mean pressure of mixture [$N\ m^{-2}$]
$\bar{P}$ dimensionless cross-sectional mean pressure, $\bar{p}/(\rho\bar{w}_0^2)$
Pr Prandtl number, ν/α
p_w partial pressure of water vapor at interface
q_i'' interfacial energy flux into air stream, [$W\ m^{-2}$]
q_l'' latent energy flux flowing into air stream [$W\ m^{-2}$]
q_s'' sensible energy flux flowing into air stream [$W\ m^{-2}$]
Re Reynolds number, $\bar{w}_0D_e/\nu$
S circumference of cross-section [m]
S^* parameter, equation (19)
Sc Schmidt number, ν/D
Sh_z local Sherwood number
T temperature [°C, K]
T_0 uniform fluid temperature at entrance [°C, K]
T_w temperature of wetted wall [°C, K]
u, v, w velocity components in the x-, y- and z-directions, respectively [$m\ s^{-1}$]
U, V, W dimensionless velocity components in the x-, y- and z-directions, respectively, $= uD_e/\nu,\ vD_e/\nu,\ w/\bar{w}_0$
v_e interfacial velocity of mixture [$m\ s^{-1}$]
$\bar{w}_0$ mean velocity at the entrance $(Z/Pr=0)$
x, y, z coordinate system [m]
X, Y, Z dimensionless coordinate system, $= x/(D_e),\ y/(D_e)\ z/(D_eRe)$.

Greek symbols

α thermal diffusivity [$m^2\ s^{-1}$]
β coefficient of thermal expansion [K^{-1}]
γ aspect ratio, a/b
ξ dimensionless vorticity in the z-direction
θ dimensionless temperature, $(T-T_0)/(T_w-T_0)$
ν kinematic viscosity [$m^2\ s^{-1}$]
ρ fluid density [$kg\ m^{-3}$]
τ_w shear stress [$N\ m^{-2}$]
ϕ relative humidity of moist air in the ambient.

Subscripts

b bulk quantity
0 condition at inlet
w condition at porous wetted wall
wall duct wall.

mined the temperature and concentration fields between vertical parallel plates via a finite-difference solution of the time dependent boundary layer equations. The negative buoyancy of the gas resulted in a downward flow along the permeable wall, while heat transfer at the other wall caused an opposing upward flow. Chang *et al.* [8] numerically investigated the natural convection heat and mass transfer in a vertical open tube. The effects of tube length and the system temperatures on the momentum, heat and mass transfer in the flow were examined in great detail. They found that the heat transfer enhancement through mass diffusion connected with film evaporation is considerable. The boundary layer forced convection flows over a flat surface with mass transfer are available in the literature [9–12]. Hanna [9] used the molar average velocity to simplify the results of isothermal diffusion in a variable molecular-weight binary gas mixture. He suggested that for diffusion in a laminar boundary layer, the constant property assumption may be a reasonable approximation, particulary if the results are evaluated at free steam conditions. Manganaro

and Hanna [10] asymptotically solved the mole fraction formulated boundary layer equation for simultaneous heat and mass transfer in a variable property binary gas mixture for both forced and free convection flows. The results showed that property variations are generally more important for free convection than for forced convection. Chow and Chung [11] studied the evaporation of water into a laminar stream of hot air and superheated steam. Results were obtained for variable thermophysical properties and constant thermophysical properties using the one-third rules. A similar problem was also examined by Schröppel and Thiele [12] for liquid-film evaporation in laminar and turbulent flows. The system of boundary layer equations was numerically solved using an implicit finite-difference method of the Hermitian type. They found that mass transfer has a pronounced impact on forced convection flow and heat transfer. For fixed convection flows, Santarelli and Foraboschi [13] examined the effects of natural convection on a laminar forced convection flow undergoing a chemical reaction. They concluded that the effects of natural convection on conversion is greater for exothermic reactions than for endothermic ones. Yan and his colleagues [14–17] numerically investigated the laminar or turbulent mixed convection flow in a vertical channel or tube under simultaneous influence of the combined buoyancy effects of the thermal and mass diffusion for an air–water vapor system. Results showed that the effects of the evaporation or condensation of water vapor on the heat transfer are rather substantial. Recently, mixed convection heat and mass transfer in horizontal ducts has been performed by Lin *et al.* [18, 19]. The buoyancy-induced secondary flow on the heat and mass transfer are examined in detail.

In spite of its importance in engineering applications, the mixed convection heat and mass transfer in vertical rectangular ducts has not been adequately studied; this motivates the present work. Consider a steady three-dimensional laminar flow in the entrance region of a vertical rectangular duct, as schematically shown in Fig. 1. A uniform axial velocity $\bar{w}_0$ is imposed at the entrance ($z = 0$) and constant wall temperature and concentration are imposed in the wetted surface at $z > 0$. One of the four vertical walls is porous and the other three are solid. The porous wall is wetted by a thin liquid water film and is maintained at a uniform temperature T_w, while the other solid walls are kept thermally insulated. As a preliminary study, the liquid film is assumed so thin that it can be treated as a boundary condition. In reality, the liquid film is of finite thickness and the movement of the liquid film may influence the characteristics of flow and heat transfer near the gas–liquid interface. In this work, the flow of moist air, with relative humidity ϕ, enters the duct from the bottom end. Due to the temperature and concentration differences between the moist air in the duct and the wetted porous wall, the forced flows would be affected by the combined buoyancy forces of thermal and mass diffusion.

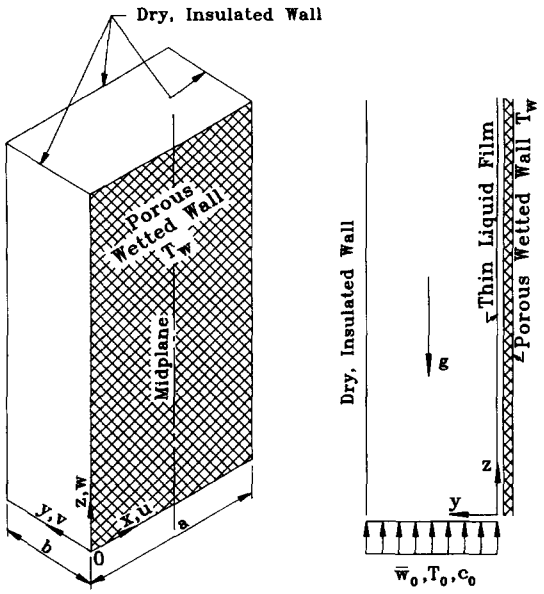

Fig. 1. Schematic diagram of the physical model.

ANALYSIS

To facilitate the analysis, an order of magnitude analysis is used to deduce the governing equations by neglecting the axial diffusion of momentum, heat and mass [20, 21]. In addition, the thermophysical properties of the mixture are assumed to be constant except for the density variation in the buoyancy term of the momentum equation for the vertical direction—they are evaluated by the one-third rule [11, 22]. A detail evaluation of the thermophysical properties is available in Fujji *et al.* [23]. In this work, the Boussinesq approximation is used to characterize the buoyancy effect [24]. The viscous dissipation and compression effects are neglected. By introducing a vorticity function in the axial direction, $\xi = \partial U/\partial Y - \partial V/\partial X$, the vorticity–velocity formulation of Navier–Stokes equations can be derived and shown as follows:

$$\nabla^2 U = \frac{\partial \xi}{\partial Y} - \frac{\partial^2 W}{\partial X \partial Z} \tag{1}$$

$$\nabla^2 V = -\left(\frac{\partial \xi}{\partial X}\right) - \frac{\partial^2 W}{\partial Y \partial Z} \tag{2}$$

$$U\frac{\partial \xi}{\partial X} + V\frac{\partial \xi}{\partial Y} + W\frac{\partial \xi}{\partial Z} + \xi\left(\frac{\partial U}{\partial X} + \frac{\partial V}{\partial Y}\right) + \left(\frac{\partial W}{\partial Y}\right)\left(\frac{\partial U}{\partial Z}\right) - \left(\frac{\partial W}{\partial X}\right)\left(\frac{\partial V}{\partial Z}\right) = \nabla^2 \xi - \left(Gr_t \frac{\partial \theta}{\partial X} + Gr_m \frac{\partial C}{\partial X}\right) \tag{3}$$

$$U\frac{\partial W}{\partial X}+V\frac{\partial W}{\partial Y}+W\frac{\partial W}{\partial Z}$$

$$=-\left(\frac{\mathrm{d}\bar{P}}{\mathrm{d}Z}\right)+(Gr_t\cdot\theta+Gr_m\cdot C)/Re+\nabla^2 W \quad (4)$$

$$U\frac{\partial\theta}{\partial X}+V\frac{\partial\theta}{\partial Y}+W\frac{\partial\theta}{\partial Z}=\left(\frac{1}{Pr}\right)\nabla^2\theta \quad (5)$$

$$U\frac{\partial C}{\partial X}+V\frac{\partial C}{\partial Y}+W\frac{\partial C}{\partial Z}=\left(\frac{1}{Sc}\right)\nabla^2 C \quad (6)$$

where $\nabla^2=\partial^2/\partial X^2+\partial^2/\partial Y^2$. It should be noted that the axial diffusion terms in equations (3)–(6) are neglected under the conditions of high Peclet numbers [25]. In the present study the symmetry condition is imposed on the midplane to reduce the computational domain. Because of the geometrical symmetry in a rectangular duct, it suffices to solve the problem in the half-region shown in Fig. 1. Therefore, the governing equations are subject to the following boundary conditions:

$$U=V=W=0 \quad \partial\theta/\partial n=\partial C/\partial n=0$$

(at solid walls) (7)

$$U=0, \quad V=V_e \qquad W=0, \quad \theta=C=1$$

(at wetted wall) (8)

$$U=\partial V/\partial X=\partial W/\partial X=\partial\theta/\partial X=\partial C/\partial X=0$$

(at the plane of symmetry) (9)

$$W=1 \quad U=V=\xi=\theta=C=0$$

(at entrance $Z=0$). (10)

Since the air–water interface is semipermeable (the solubility of air in water is negligibly small and air velocity in the y-direction is stationary at the interface), the evaporating velocity of the mixture at the wetted surface is evaluated by Burmeister [26]

$$V_e=-(c_w-c_0)\cdot(\partial C/\partial Y)/[Sc(1-c_w)]. \quad (11)$$

According to Dalton's law and the state equation of ideal gas mixture, the interfacial mass fraction of water vapor can be calculated by

$$c_w=p_w M_v/[p_w M_v+(p-p_w)M_a] \quad (12)$$

where p_w is the saturated water vapor pressure at the wetted wall. The overall mass flow rate at every axial location must be balanced in the duct flow:

$$\int_0^{(1+\gamma)/2\gamma}\int_0^{(1+\gamma)/4} W\,\mathrm{d}X\,\mathrm{d}Y$$

$$=\frac{(1+\gamma)^2}{8\gamma}+\int_0^Z\int_0^{(1+\gamma)/4} V_e\,\mathrm{d}X\,\mathrm{d}Z. \quad (13)$$

This equation is employed to deduce the axial pressure gradient in equation (4). After obtaining the developing velocity, temperature and concentration fields along the axial direction, the computation of the local friction coefficient, Nusselt number and Sherwood number are of practical interest. The dimensionless friction factor is defined as

$$fRe=-2(\overline{\partial W/\partial n})_{wall}. \quad (14)$$

The total heat from the wetted surface can be expressed as [17]

$$q_t''=q_s''+q_l''=-k\left(\frac{\partial T}{\partial y}\right)_w-\left[\frac{\rho Dh_{fg}}{1-c_w}\right]\cdot\left(\frac{\partial c}{\partial y}\right)_w \quad (15)$$

where q_t'', q_s'' and q_l'' denote the interfacial heat flux, sensible heat flux and latent heat flux, respectively. The locally averaged Nusselt numbers over the porous wetted wall can then be written as

$$Nu_z=Nu_s+Nu_l \quad (16)$$

where Nu_s and Nu_l can be evaluated by considering the overall energy balance for axial length $\mathrm{d}Z$

$$Nu_s=\left(\frac{Pr}{1-\theta}\right)\cdot\left(\frac{\partial\theta_b}{\partial Z}\right) \quad (17)$$

$$Nu_l=\left(S^*\frac{Sc}{1-\theta_b}\right)\cdot\left(\frac{\partial C_b}{\partial Z}\right) \quad (18)$$

where S^* signifies the importance of the energy transport through species diffusion relative to that through thermal diffusion

$$S^*=\rho Dh_{fg}(c_w-c_0)/[k(T_w-T_0)]. \quad (19)$$

For a low mass transfer rate at the interface, a mass transfer coefficient h_m based on overall mass balance is defined as

$$\rho h_m a\Delta z\cdot(c_w-c_b)=\rho A\bar{w}_0\Delta c(1-c_w). \quad (20)$$

The local Sherwood number Sh then becomes

$$Sh_z=h_m D_e/D=[Sc(1-c_w)/(1-c_b)]\cdot(\partial C_b/\partial Z). \quad (21)$$

SOLUTION METHOD

The present work was solved numerically by a vorticity–velocity method for three-dimensional parabolic flow [24]. For a given condition, the field solutions are calculated by a marching technique based on the Du Fort–Frankel scheme [27]. Details of the solution procedure have been described elsewhere [18, 19] and are not repeated herein.

To verify the proposed numerical scheme, a series of program tests were performed. First the limiting case of purely forced convection in a square duct was obtained. The predicted Nu was found to be in excellent agreement with that of Neti and Eichhorn [28]. Then, the mixed convection heat and mass transfer in a horizontal square duct was computed. The predicted local Nusselt number was compared with

Table 1. Comparison of local Nusselt number Nu_z for various grid arrangements for Case II with $\gamma = 1$

$M \times N$ / $\Delta Z/Pr$	Z/Pr 0.00598	0.0125	0.0252	0.0502	0.101	0.198
12×24 ($1 \times 10^{-4} - 3 \times 10^{-3}$)	39.014	30.137	24.498	20.815	18.469	16.688
20×40 ($1 \times 10^{-4} - 3 \times 10^{-3}$)	38.272	29.872	24.383	20.755	18.445	16.735
20×40 ($2 \times 10^{-5} - 3 \times 10^{-3}$)	38.607	29.995	24.438	20.781	18.454	16.718
30×60 ($1 \times 10^{-4} - 3 \times 10^{-3}$)	38.019	29.751	24.305	20.691	18.408	16.805

that of Lin *et al.* [18, 19] and it is found that the local Nu agrees within 2% at all axial locations. Finally, to examine the grid-dependence of the numerical results, a numerical experiment was performed with various grid distributions in a cross-section plane ($M \times N$) and an axial step size ($\Delta Z/Pr$). In this work, the grid lines were uniformly arranged in the cross-plane, but non-uniformly arranged in the axial direction for the uneven variations of field properties in the entrance region. Table 1 presents the results of the local Nu_z for four grid systems. It is found from Table 1 that the differences in local Nu_z calculated using either $M \times N = 20 \times 40$ or 30×60 ($\Delta Z/Pr = 1 \times 10^{-4} - 3 \times 10^{-3}$) are always within 1%. Furthermore, the deviations in local Nu_z calculated using either $M \times N(\Delta Z/Pr) = 20 \times 40(2 \times 10^{-5} - 3 \times 10^{-3})$ or $20 \times 40(1 \times 10^{-4} - 3 \times 10^{-3})$ are less than 1%. Through these program tests, the adopted solution scheme was considered to be suitable for the present study.

RESULTS AND DISCUSSION

The preceding analysis indicates that the mixed convection heat and mass transfer in vertical rectangular ducts depends on Re, Pr, Sc, Gr_t, Gr_m and γ. It should be recognized herein that not all the values of the nondimensional groups can be arbitrarily assigned. Some of them (i.e. Sc, Gr_t and Gr_m) are interdependent for a given mist air under certain specific conditions. Instead of physical parameters—the wetted wall temperature, the relative humidity of the ambient air and the inlet Reynolds number—are picked as the independent variables. In the present study, to focus on the transport phenomena of heat and mass diffusion: the unsaturated moist air at the inlet is fixed at 20°C and 1 atm, the relative humidity of the inlet mixture is chosen to be 10, 50 or 90%, the porous wetted wall is kept at a uniform temperature 40 or 60°C and the through-flow Reynolds number at the inlet, Re, is assigned to have a value of 1000 or 2000. Based on the above specified conditions, the dimensionless parameters can then be obtained for several cases, indicated in Table 2. Additionally, in order to investigate the effects of the aspect ratio, the aspect ratio γ is chosen to have value of 0.5, 1.0 or 2.0. Numerical solutions were obtained for the distributions of velocity, temperature and concentration profiles, the local friction factor, the Nusselt number and the Sherwood number.

Figure 2 shows the axial velocity distributions in a channel cross-section at different Z/Pr by using the lines of equal velocity W for cases II and V. To assess the influence of buoyancy effects on the mixed convection flow, the results of the limiting case of purely forced convection are also included in Fig. 2. Since the flow is symmetric with respect to the middle plane ($X = 0.5$), results need only be presented for the left half of the duct. Near the entrance ($Z/Pr = 0.002$), the contours of the axial velocity for the greater velocity of W in the central core are not shown, since the velocities are fairly uniform there. Additionally, the buoyancy effects are still weak and the iso-velocity distributions are seen to be nearly symmetric with respect to both $X = 0.5$ and $Y = 0.5$ lines. As the flow develops, the velocity in the core region is accelerated due to the entrance effect. It is clearly seen that in Fig. 2 the velocity profiles develop gradually from the uniform distributions at the inlet to the parabolic ones in the fully developed region, a situation normally found in laminar internal flows. In the case of

Table 2. Values of major parameters for various cases

Case	Re	T_w[°C]	T_0 [°C]	ϕ [%]	Pr	Sc	Gr_t	Gr_m
I	2000	40	20	10	0.703	0.592	109840	44200
II	2000	40	20	50	0.703	0.592	109960	38590
III	2000	40	20	90	0.703	0.592	110080	32930
IV	2000	60	20	10	0.703	0.592	193880	112990
V	2000	60	20	50	0.703	0.592	194060	108100
VI	2000	60	20	90	0.703	0.592	194240	103170
VII	1000	40	20	50	0.703	0.592	109960	38590

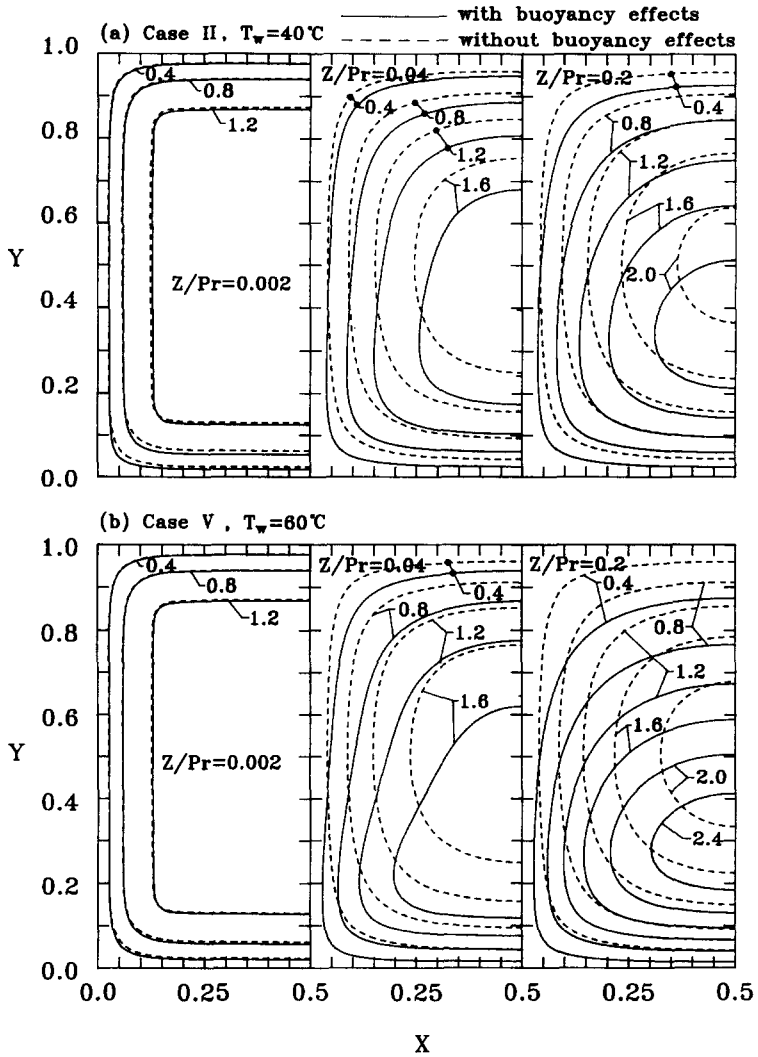

Fig. 2. The iso-velocity contours at certain axial locations for cases II and V, for $\gamma = 1$.

purely forced convection, the contours of the axial velocity are symmetric with respect to the line $Y = 0.5$ through the duct. But as the buoyancy effects are taken into account, the velocity profiles are gradually distorted by the combined buoyancy forces after a certain axial location. Furthermore, the peak axial velocity moves towards the wetted wall ($Y = 0$) as the air moves downstream. This is readily explained by the fact that the value of $(Gr_t\theta + Gr_m C)/Re$ is large near the wetted wall which results in significant buoyancy-aiding effects. A comparison of Fig. 2(a) and (b), indicates that an increase in wetted wall temperature T_w (case V) results in a higher axial velocity and the distortion of velocity profiles is more significant. This phenomenon conforms with a greater amount of water vapor evaporating into the air stream for a higher T_w and larger combined buoyancy forces through thermal and mass diffusion.

Shown in Figs. 3 and 4 are the contours of the iso-concentration and isotherms at different axial locations, respectively. It is of interest to note that both θ and C develop in a very similar way. This is simply because the Pr and Sc in the gas flow are of the same order ($Pr = 0.7$ and $Sc = 0.6$). Careful inspection, however, discloses that the mass-fraction boundary layers develop a little more rapidly than the temperature boundary layers. This is simply due to the fact that Pr is slightly larger than Sc in the flow ($Pr = 0.7$ and $Sc = 0.6$). In line with the wall heating and liquid film evaporation, the temperature and mass fraction in the central portion of the channel increase gradually as the moist air goes downstream. It is also clear in Figs. 3 and 4 that relative to the pure forced convection results, the developments of temperature and concentration profiles are slower for the mixed convection case. This is simply due to the fact that the flow near the heated wall is continuously accelerated by the aiding buoyancy effects along the axial direction, enhancing the heat and mass transfer in the z-direction and hence, decreasing the advancement of heat and mass transfer in the transverse directions. This implies that the temperature and concentration

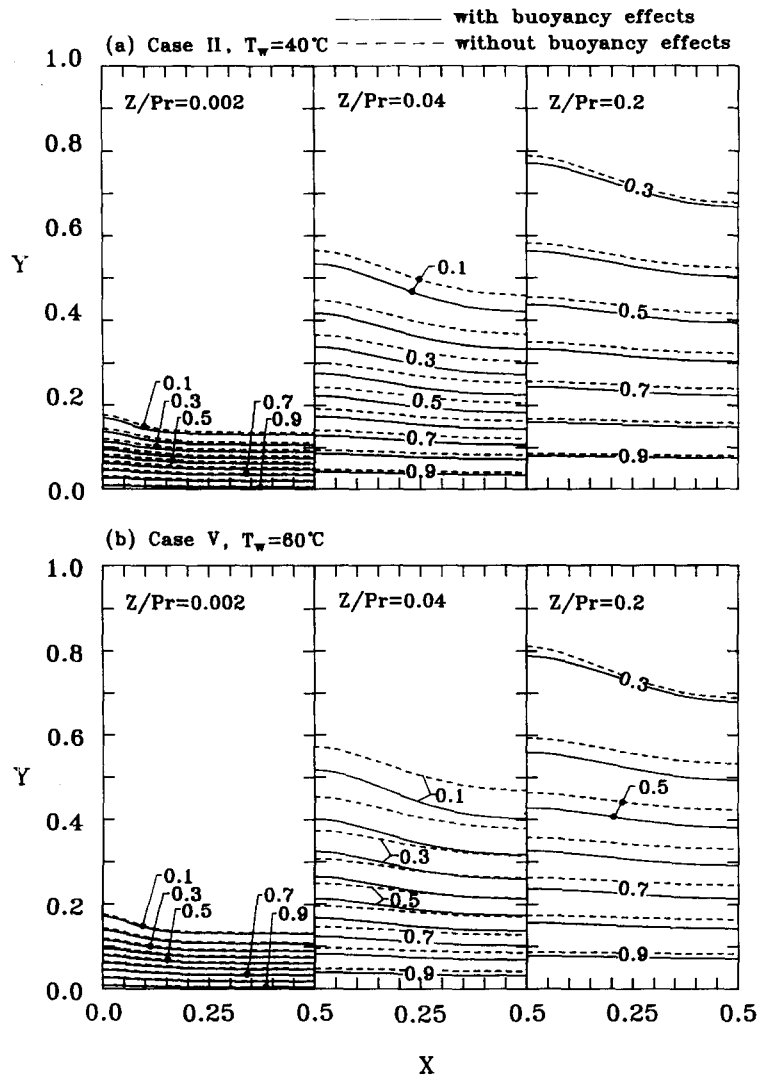

Fig. 3. The iso-concentration contours at certain axial locations for cases II and V, for $\gamma = 1$.

gradients at the wetted wall are lower for pure convection, and consequently, a lower wall heat flux due to sensible and latent heat exchanges is found for the results without buoyancy effects. As the fluid flows through the duct, the discrepancy of temperature and concentration between the side wall and the central portion becomes more significant. This is attributed to the side-wall hydrodynamic buoyancy-layer development. Although not shown in the results presented in Figs. 3 and 4, it was found in separate numerical runs that the temperature and concentration gradients at $Y = 0$ are a little steeper for a system with a higher T_w, which in turn causes a higher latent and sensible heat transfer. This result is reflected by the distributions of Nu_l and Nu_s in Fig. 5.

To study the relative contributions of heat transfer through sensible and latent heat exchanges in the flow, three kinds of Nusselt numbers are presented in Fig. 5. An overall comparison of the solid (with buoyancy effects) and dashed (without buoyancy effects) curves for the corresponding cases indicates the buoyancy effects have a substantial augmentation in heat and mass transfer. For pure forced convection cases, it is observed that the curves of Nu_s and Nu_l for cases II′ and VII′ with different values of Re collapse to a single curve. This is because terms in the momentum equation (4) can be neglected. Therefore, the velocity and temperature developments are identical for various Re(scaling with Z/Re). It is also noted that for pure forced convection a larger Nu_s is noted for a lower T_w by comparing case II′ and V′. This is clearly related to the weaker evaporation rate for a lower wall temperature T_w. But in Fig. 5(b), the trend is reversed, i.e. the Nu_l is greater for a higher T_w. This results from the greater latent heat transfer transport connected with the larger water evaporation from the wetted wall.

Turning to the case of mixed convection, a comparison of case II and V indicates that a larger Nu_s is noted for a higher T_w. This is expected because a

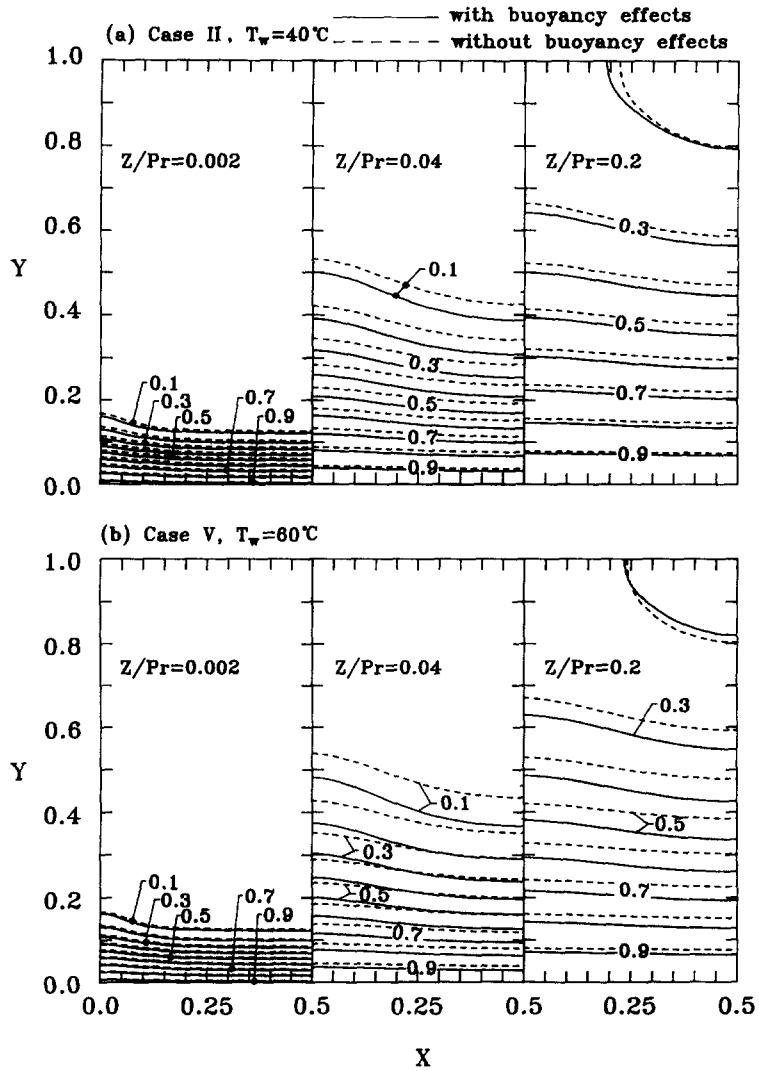

Fig. 4. The isotherm contours at certain axial locations for cases II and V, for $\gamma = 1$.

higher T_w causes larger buoyancy effects. The influence of Reynolds number Re on the local Nu_s is also included in Fig. 5(a). A comparison of cases II and VII shows that the sensible heat transfer Nu_s is more effective for the flow with a lower Re owing to the larger buoyancy effects (higher Gr_t/Re and Gr_m/Re). Due to the reasons discussed in the case of pure forced convection, larger Nu_l is observed for a higher T_w. An overall inspection of Fig. 5(a)–(b) depicts that the heat transfer due to latent heat transport is much more effective than that due to sensible heat transport. In Fig. 5(c), Nu_z, the sum of Nu_s and Nu_l, is presented.

The effects of T_w and Re on the local Sherwood number Sh_z are presented in Fig. 6(a). In Fig. 6(a), the distributions of Sh_z resemble those of Nu_s in Fig. 5(a). This is because in this study the Prandtl number Pr and Schmidt number Sc are of the same order of magnitude. It is clearly seen in Fig. 6(a) that a larger Sh_z is found for the flow with a higher T_w (by comparing case II and V); this is due to the larger combined buoyancy effects (i.e. Gr_t/Re and Gr_m/Re). Comparison of the results between the curves of $Re = 2000$ (case II) and $Re = 1000$ (case VII) shows that the effect of decreasing Re is to increase Sh_z. This can be explained from the fact that a lower Re causes a smaller binary diffusion effect and a thinner concentration buoyancy layer, relative to the flow boundary layer. This results in a larger concentration gradient at the wetted wall and hence, a larger mass transfer rate and Sherwood number. Moreover, the result with buoyancy effects has a larger Sh_z than that of purely forced convection. The distributions of friction factor fRe are given in Fig. 6(b). The local fRe with buoyancy effects is always larger than that without buoyancy effects. Additionally, the case with a higher wall temperature shows a greater friction factor.

It is interesting to examine the effect of the relative humidity of the ambient moist air on the transport of latent heat. The local latent heat Nusselt number Nu_l with various ϕ is shown in Fig. 7. As seen in Table 2, a lower ϕ corresponds to a higher Gr_m. For a larger Gr_m, heat transfer is strongly affected by species

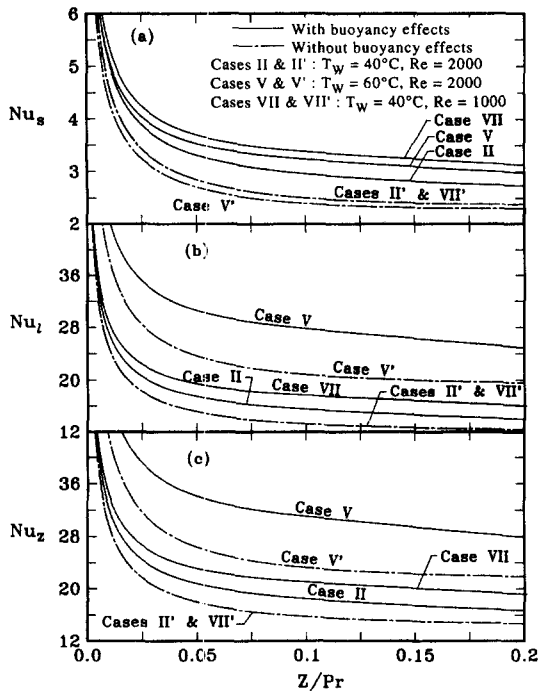

Fig. 5. The axial variations of Nu_s, Nu_l and Nu_z for cases II, V and VII.

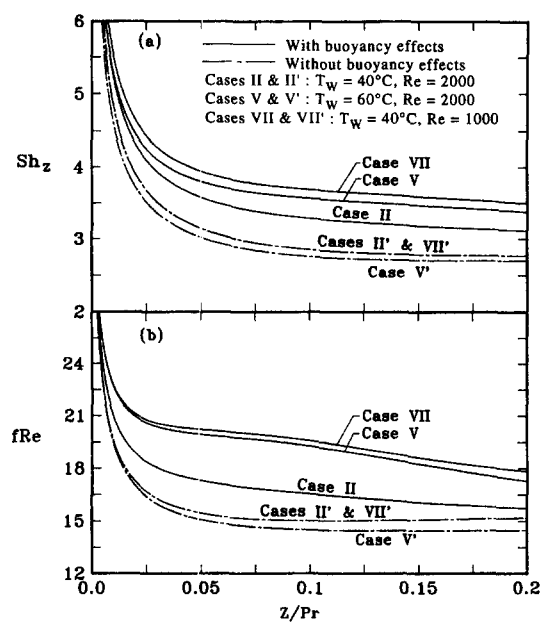

Fig. 6. The axial variations of Sh_z and fRe for cases II, V and VII.

diffusion. This is because the species diffusion mechanism is more effective at lower concentration levels. Moreover, the influence of ϕ on Nu_l is more pronounced for a flow with a lower T_w. This confirms the results of a previous study by Lin *et al.* [17]. This obviously indicates that the vaporization of the liquid film is substantially reduced, relative to the original

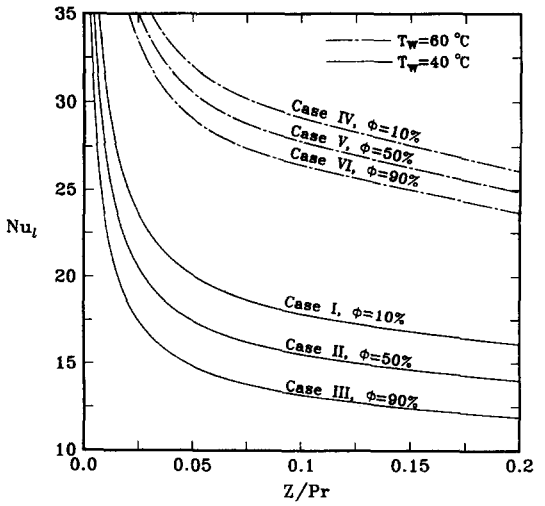

Fig. 7. Effects of wall temperature T_w on the axial variations of Nu_l.

evaporation, as the relative humidity increases. This trend is strongest for a low T_w, wherein the driving potential for mass transfer Gr_m is smaller, and the variation of Gr_m with relative humidity (in absolute change and percentage) is smaller. This trend is apparent if the change in Gr_m with T_w is checked, as given in Table 2.

To study the effect of the aspect ratio γ on the flow pattern, Fig. 8(a)–(c) presents the iso-velocity distributions at $Z/Pr = 0.2$ for $\gamma = 0.5$, 1, and 2.0, respectively. It is clear that the maximum velocity is greater for the duct with the smaller γ. This is due to the fact that the temperature difference along the Y-direction is higher for smaller γ, which causes a greater buoyancy force in the fluid flow.

The effect of the channel aspect ratio (γ) on the local Nu_z, Sh_z and fRe are of practical interest. The axial variations of Nu_z, Sh_z and fRe for aspect ratio $\gamma = 0.5$, 1 and 2.0 are shown in Fig. 9. It is clearly shown in Fig. 9(a) and (b), that within the range of the aspect ratio under consideration, larger Nu_z and Sh_z are noted for a system with a greater γ. This is due to the wider porous wetted wall for a system having a larger γ, which in turn, causes a greater film evaporation into gas flow. It is noted that the fRe of the wider and more slender duct is greater than that of the square duct for the flow with the same Re. Comparison of the results between $\gamma = 2.0$ and $\gamma = 0.5$ for all cases shows that a larger fRe is observed for $\gamma = 2.0$ near the entrance region, but the trend is reversed in the downstream direction.

CONCLUDING REMARKS

The nature of combined buoyancy effects of thermal and mass diffusion on laminar forced convection in the thermal entrance region of vertical rectangular ducts has been studied. The effects of the wetted wall

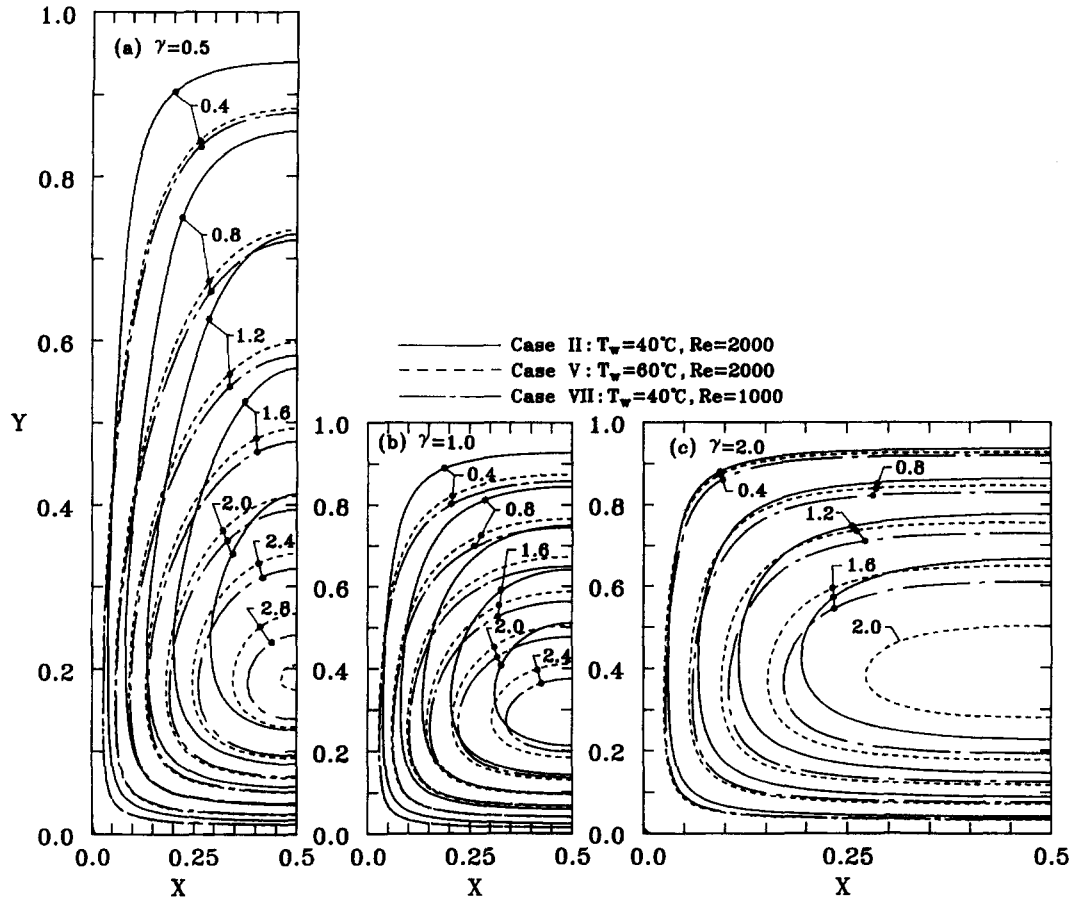

Fig. 8. Effects of aspect ratio γ on the isovelocity contours at the exit of duct.

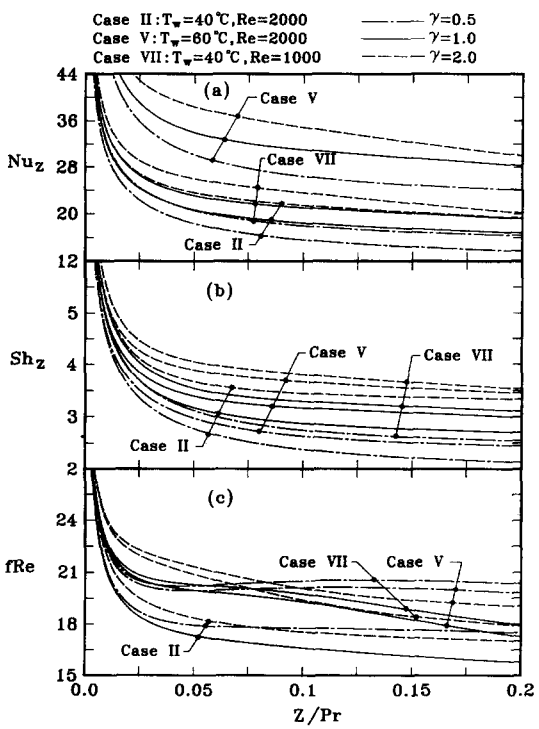

Fig. 9. Effects of aspect ratio γ on the axial variations of Nu_z, Sh_z and fRe.

temperature, the Reynolds number of the flow, the relative humidity of the moist air in the ambient and the aspect ratio of the duct on the transfer of momentum, heat and mass in the flow, were examined in detail. Following is a brief summary of the major results:

(1) Heat transfer along the porous wetted wall is dominated by the transport of latent heat in association with the vaporization of the water film.

(2) An increase in ϕ results in a decrease in Nu_l under the same wall temperature T_w.

(3) The buoyancy forces cause an enhancement in heat and mass transfer. The extent of the augmentation increases with an increased in T_w or a decrease in Re, compared with the corresponding results of forced convection.

(4) Higher Nu_z and Sh_z are observed for a system with a greater aspect ratio γ of the rectangular duct.

(5) The effects of film evaporation along the vertical wall on the Nusselt number Nu_z is significant. For case V (T_w = 60°C), the Nu_z is nine times the value without film vaporization.

Acknowledgement—The financial support of this work by the National Science Council, Republic of China, through contract NSC84-2212-E-211-003, is greatly appreciated.

REFERENCES

1. Somers, E. V., Theoretical considerations of combined thermal and mass transfer from a vertical flat plate. *ASME Journal of Applied Mechanics*, 1956, **23,** 295–301.
2. Mather, W. G., Madden, A. J. and Piret, E. L., Simultaneous heat and mass transfer in free convection. *Industrial Engineering Chemistry*, 1957, **49,** 961–968.
3. Gill, W. N., Casal, E. D. and Zeh, D. W., Binary diffusion and heat transfer in laminar free convection boundary layers on a vertical plate. *International Journal of Heat and Mass Transfer*, 1965, **8,** 1135–1151.
4. Saville, D. A. and Churchill, S. W., Laminar free convection in boundary layers near horizontal cylinders and vertical asymmetric bodies. *Journal of Fluid Mechanics*, 1967, **29,** 391–397.
5. Saville, D. A. and Churchill, S. W., Simultaneous heat and mass transfer in free convection boundary layers. *AIChE Journal*, 1970, **16,** 268–273.
6. Soundalgekar, V. M. and Ganesan, P., Finite difference analysis of transient free convection with mass transfer on an isothermal vertical flat plate. *International Journal of Engineering Science*, 1981, **19,** 757–770.
7. Lee, T. S., Parikh, P. G., Acrivos, A. and Bershader, D., Natural convection in a vertical channel with opposing buoyancy forces. *International Journal of Heat and Mass Transfer*, 1982, **25,** 499–511.
8. Chang, C. J., Lin. T. F. and Yan, W. M., Natural convection flows in a vertical open tube resulting from combined buoyancy effects of thermal and mass diffusion. *International Journal of Heat and Mass Transfer*, 1986, **29,** 1543–1552.
9. Hanna, O. T., Diffusion in the laminar boundary layer with a variable density. *A.I.Ch.E. Journal*, 1965, **11,** 706–712.
10. Manganaro, J. L. and Hanna, O. T., Simultaneous energy and mass transfer in the laminar boundary with large mass transfer rates toward the surface. *A.I.Ch.E. Journal*, 1970, **16,** 204–211.
11. Chow, L. C. and Chung, J. N., Evaporation of water into a laminar stream of air and superheated steam. *International Journal of Heat and Mass Transfer*, 1983, **26,** 373–380.
12. Schröppel, J. and Thiele, T. F., On calculation of momentum heat and mass transfer in laminar and turbulent boundary layer flows along a vaporizing liquid film. *Numerical Heat Transfer*, 1983, **6,** 475–496.
13. Santarelli, F. and Foraboschi, F. P., Heat transfer in laminar mixed convection in a reacting fluid. *Chemical Engineering*, 1973, **6,** 59–68.
14. Yan, W. M., Tsay, Y. L. and Lin, T.F., Simultaneous heat and mass transfer in laminar mixed convection flows between vertical parallel plates with asymmetric heating. *International Journal of Heat Fluid Flow*, 1989, **10,** 262–269.
15. Yan, W. M and Lin, T. F., Effects of wetted wall on laminar mixed convection heat transfer in a vertical channel. *J. Thermophysics and Heat Transfer*, 1989, **3,** 94–96.
16. Yan, W. M., Turbulent mixed convection heat and mass transfer in a wetted channel. *ASME Journal of Heat Transfer*, 1995, **117,** 229–233.
17. Lin, J. F., Chang, C. J. and Yan. W. M., Analysis of combined buoyancy effects of thermal and mass diffusion on laminar forced convection heat transfer in a vertical tube. *ASME Journal of Heat Transfer*, 1988, **110,** 337–344.
18. Lin, T. N., Chou, F. C., Yan, W. M. and Tzeng, P. Y., Combined buoyancy effects of thermal and mass diffusion on laminar forced convection in the thermal entrance region of horizontal square ducts. *Canadian Journal of Chemical Engineering*, 1992, **70,** 681–689.
19. Lin, J. N., Tzeng, P. Y., Chou, F.C. and Yan. W. M., Convective instability of heat and mass transfer for laminar forced convection in the thermal entrance region of horizontal rectangular channels. *International Journal of Heat Fluid Flow*, 1992, **13,** 250–280.
20. Incropera, F. P. and Schutt, J. A., Numerical simulation of laminar mixed convection in the entrance region of horizontal rectangular ducts. *Numerical Heat Transfer*, 1985, **8,** 707–729.
21. Mahaney, H. V., Incropera, F. P. and Ramadhyani, S., Development of laminar mixed convection flow in a horizontal rectangular duct with uniform bottom heating. *Numerical Heat Transfer*, 1987, **12,** 137–155.
22. Hubbard, G. L., Denny, V. E. and Mills, A. F., Droplet evaporation: effects of transients and variable properties. *International Journal of Heat and Mass Transfer*, 1975, **18,** 1003–1008.
23. Fujji, T., Kato, Y. and Mihara, K., Expression of transport and thermodynamic properties of air, steam and water. *Sei. San Ka Gaku Ken Kyu Jo*, Report no. 66, Kyu Shu Dai Gaku, Kyu Shu, Japan, 1977, pp. 81–95.
24. Ramakrishna, K., Rubin, S. G. and Khosla, P. K., Laminar natural convection along vertical square ducts. *Numerical Heat Transfer*, 1982, **5,** 59–79.
25. Shah, R. K. and London. A. L., *Laminar Flow Forced Convection in Duct*. Academic Press, New York, 1978.
26. Burmeister, L. C., *Convective Heat Transfer*. McGraw-Hill, New York, 1983, pp. 170–174.
27. Roche, P. J., *Computational Fluid Dynamics*. Reinhold, New York, 1971, pp. 61–64.
28. Neti, S. and Eichhorn, R., Combined hydrodynamic and thermal development in a square duct. *Numerical Heat Transfer*, 1983, **6,** 497–510.